Received: 6 December 2022 | Revised: 7 March 2023 | Accepted: 12 July 2023

DOI: 10.1002/cyto.a.24778

ORIGINAL ARTICLE

ISAC CYTOMETRY Journal of Quantitative Cell Science PART A

Effect of pulsed laser parameters on photoacoustic flow cytometry efficiency in vitro and in vivo

Oleg V. Grishin[1] | Natalia A. Shushunova[1] | Daniil N. Bratashov[1] | Ekaterina S. Prikhozhdenko[1] | Roman A. Verkhovskii[1] | Anastasiia A. Kozlova[1] | Arkady S. Abdurashitov[2] | Olga A. Sindeeva[2] | Anatoly S. Karavaev[1,3,4] | Danil D. Kulminskiy[3,5] | Evgeny V. Shashkov[6] | Olga A. Inozemtseva[1] | Valery V. Tuchin[1,7,8,9]

[1]Science Medical Center, Saratov State University, Saratov, Russia

[2]A.V. Zelmann Center for Neurobiology and Brain Rehabilitation, Skolkovo Institute of Science and Technology, Moscow, Russia

[3]Laboratory of Nonlinear Dynamics Modeling, Saratov Branch of the Institute of Radio-Engineering and Electronics of Russian Academy of Sciences, Saratov, Russia

[4]Department of Innovative Cardiological Information Technology, Institute of Cardiological Research, Saratov State Medical University, Saratov, Russia

[5]Scientific Center for Information Technologies and Artificial Intelligence, Sirius University of Science and Technology, Sochi, Russia

[6]Pico-Femtoseconds Laser Laboratory, Photoelectronics Department, Prokhorov General Physics Institute of the Russian Academy of Sciences, Moscow, Russia

[7]Laboratory of Laser Molecular Imaging and Machine Learning, Tomsk State University, Tomsk, Russia

[8]Institute of Precision Mechanics and Control, FRC "Saratov Scientific Centre of the Russian Academy of Sciences", Saratov, Russia

[9]Bach Institute of Biochemistry, FRC "Fundamentals of Biotechnology of the Russian Academy of Sciences", Moscow, Russia

Correspondence
Daniil N. Bratashov, Science Medical Center, Saratov State University, 83 Astrakhanskaya Str., Saratov 410012, Russia.
Email: bratashovdn@info.sgu.ru

Funding information
Council on grants of the President of the Russian Federation, Grant/Award Number: MK-4273.2021.1.4; Government of the Russian Federation, Grant/Award Number: 14.Z50.31.0044

Abstract

Photoacoustic flow cytometry is one of the most effective approaches to detect "alien" objects in the bloodstream, including circulating tumor cells, blood clots, parasites, and emboli. However, the possibility of detecting high-amplitude signals from these objects against the background of blood depends on the parameters of the laser pulse. So, the dependencies of photoacoustic signals amplitude and number on laser pulse energy (5–150 μJ), pulse length (1, 2, 5 ns), and pulse repetition rate (2, 5, 10 kHz) for the melanoma cells were investigated. First, the PA responses of a melanoma cell suspension in vitro were measured to directly assess the efficiency of converting laser light into an acoustic signal. After it, the same dependence with the developed murine model based on constant rate melanoma cell injection into the animal blood flow was tested. Both in vivo and in vitro experiments show that signal generation efficiency increases with laser pulse energy above 15 μJ. Shorter pulses, especially 1 ns, provide more efficient signal generation as well as higher pulse rates. A higher pulse rate also provides more efficient signal generation, but also leads to overheating of the skin. The results show the limits where the photoacoustic flow cytometry system can be effectively used for the detection of circulating tumor cells in undiluted blood both for in vitro experiments and for in vivo murine models.

KEYWORDS
in vivo flow cytometry, laser pulse length, photoacoustic flow cytometry, photoacoustics

1 | INTRODUCTION

Flow cytometry is one of the most widely used research methods in biology and medicine. However, invasive sampling of small blood volumes (usually ≤10 mL) results in missing rare biomarkers, especially in the early stages of the disease [1]. Thus, when analyzing extremely rare cell populations in flow cytometry, the collected blood volume contains at best single target cells. With an unfortunate set of circumstances, they may not be present in the sample volume at all. In comparison, in vivo flow cytometry is able to analyze a much larger volume of whole blood [1–4]. For instance, the number of circulating tumor cells (CTCs) in a patient's blood at early-stage cancer [5] is so low that the typical volume of blood samples extracted for in vitro tests can skip almost all of such cells [6, 7]. The sensitivity of the in vivo flow cytometry method can reach a single cell per liter level [1, 8], which is at least 1–2 orders of magnitude superior to other available methods.

Currently, there are several common approaches to the construction of in vivo cytometry systems, including photoacoustic flow cytometry (PAFC) [8–11], ultrafast scanning photoacoustic system [10, 12, 13], fluorescence [14–18], fluorescence imaging [19–23], scattering [24–27], diffuse fluorescence [7, 28–31], stimulated Raman scattering [32] among other cytometry methods.

PAFC is one of the most successful approaches to the development of in vivo flow cytometry systems. The detection of melanoma cells in blood [14, 17], lymphatic vessels [33], and cerebrospinal fluid [34] has been described in both in vivo and in vitro studies. Various in vivo flow cytometry techniques allow detection of CTCs [35], blood clots [36, 37], sickle cells [38], malaria parasites [39], bacteria causing blood infections [40], and other emboli [41] in the patients' blood non-invasively. When using PAFC to detect melanoma cells, strong intrinsic absorption allows them to be seen even at a considerable depth against the background of the red blood cells (RBC) signal.

Several works describe a set of parameters required to build an effective photoacoustic tomography system [42] and necessary approaches to reduce its cost [43, 44]; however, requirements for components designed to build a dynamic PAFC system are still under active investigation. The correct choice of laser components and their parameters is crucial as it affects the performance of the entire PAFC system, its cost, patient safety, and the reliability and scientific/diagnostic validity of the received signals. The required combination of pulse width, repetition rate, and pulse energy is usually difficult to implement in modern laser systems designs, which significantly affects the cost of the device.

The idea of detecting circulating melanoma cells is based on the intrinsic contrast of melanin grains. Better light-absorbing melanin grains generate a nonlinear photoacoustic (PA) signal comparable to or stronger than the linear PA signal from erythrocyte hemoglobin. However, obtaining a nonlinear signal requires a relatively high-energy density at the depth of the vessel. The creation of such a high-energy density is complicated by the fact that optical radiation is strongly scattered by biological tissues and blood. The maximum energy of the laser pulse is limited from above by the energy density on the skin surface, regulated by laser safety standards. All these processes depend on the parameters of laser radiation; therefore, it is necessary to find such a combination of them that will lead to the most efficient generation of PA signals in the vessel. The main requirement is to deliver sufficient laser power to the cells inside the blood vessel without overheating the skin [8]. There is a thin balancing on the verge of skin overheating and the beginning of the effective generation of PA signals at a vessel's depth. The choice of right laser parameters shifts the balance in the right direction and increases the likelihood of detecting abnormal cells in the bloodstream at the safe laser power.

The typical approach to build a PAFC system is to use a high-energy pulsed laser with a pulse width of several nanoseconds. Usually, vessel parts near the skin are chosen: either on the back of the wrist or over the human cubital vein [1] or jugular vein on the patient's neck [45]. It is necessary to work at a wavelength falling into the transparency window of biological tissue [46]. It is better to use a wavelength with minimal absorption of oxy- and deoxyhemoglobin. However, this makes it challenging to find the vessel without a PA signal from RBCs. On the one hand, a large absorption of hemoglobin at a certain wavelength leads to the fact that even a nonlinear signal from melanin grains will be lost, since the concentration of melanin is much lower compared to hemoglobin. On the other hand, if a wavelength is chosen at which hemoglobin absorbs weakly, the blood vessel may not be detected. Thus, a good balance is needed: a small but sufficient absorption of hemoglobin for navigation is realized in the transparency windows of the biological tissue in the near-IR range [13].

For safety reasons, laser radiation's energy density and power density should not exceed safety limits to prevent skin damage. For laser wavelength 1064 nm, power density should not exceed 1 W/cm^2 for a long exposure time, and energy density should not be larger than 100 mJ/cm^2 for a single pulse [47]. Such a requirement is mandatory for use in humans; however, these limits are discussed as being too low for typical nanosecond pulsed lasers. Several researchers have already shown that the actual skin damage level for long-term exposure is around 0.5–1 J/cm^2 [48, 49].

The volume of the detected area should not be too large, otherwise, the signal of melanin-rich cells will be lost against the background of the RBCs signal. On the other hand, a beam profile must be achieved that will overlap the cross-section of the vessel as much as possible so that the CTCs cannot pass by the region to be detected [50]. At the typical blood flow velocities inside the human wrist vessels ~12 cm/s [1], the pulse repetition rate should be at least 100 Hz to avoid cells passing between the pulses undetected. The pulse repetition frequency is also above-limited by the overheating of the light-absorbing skin at the measurement site and usually should not exceed units of kHz.

The dependence of the PA signal on the pulse energy was studied earlier by several research groups [8, 35, 51]. The pulse width influence on the generated PA signal amplitude has been partially investigated in vivo by Zharov et al. [8]. The signals of RBC, melanoma cells, and melanosomes were measured at three laser pulse widths: 0.8 ns, 5 ns, and 10 ns. These experiments showed an increase in the PA

signal intensity by a factor of 1.5 at 0.8 ns pulse width compared to 10 ns. An increase in the amplitude of the PA signal with a decrease in the pulse duration from 45 ns to 4.5 ns was also shown in experiments with a suspension of carbon dust particles [52].

It is important to obtain the dependence of the PA signal amplitude (acoustic pressure fluctuations converted into electrical signals by the ultrasonic sensor) on the laser system parameters (pulse energy, pulse repetition rate, and pulse width at different combinations) to model and develop new systems. However, the amplitudes of individual PA responses from cells are naturally random, depending on many uncontrolled factors. Since the pigmentation of an individual melanoma cell can differ up to 10 times [53], it is crucial to develop a methodology that allows assessing PA responses on large ensembles of cells (at least 10^3). Nonetheless, statistical analysis for recorded signal sequences reveals well visible trends and dependencies. Here we analyze the influence of pulse energy, pulse repetition rate, and pulse width on the statistical distribution of PA signals from B16F10 melanoma cells.

2 | MATERIALS AND METHODS

2.1 | The PAFC system description

In both PAFC systems (Figure 1), a near-infrared ytterbium-fiber laser (model YLPP-1-150 V-30, IPG Photonics, Russia) with the following parameters: wavelength, 1064 nm; pulse width, 1, 2, and 5 ns; pulse repetition rate from 2 kHz and pulse energy up to 300 μJ at 1 ns pulse width was used. Approximately 70% of the nominal laser pulse energy reached the sample (measured in a defocused beam behind the objective). The wedge beam splitter reflected a small portion of the light to the fast p-i-n photodiode (BPW34, Vishay Semiconductor) with a custom amplifier converting diode photocurrent into voltage pulses for acquisition triggering of an analog-to-digital converter (ADC) board. The continuous wave pilot laser with a wavelength of 532 nm (CPS532-C2, Thorlabs) with a harmonic beam splitter (HBSY11, Thorlabs) was collimated collinearly with the main laser beam to provide aiming help for the in vivo experiments. Data acquisition in all experiments was performed with 500 MS/s 12-bit Waveform Digitizer for PCI Express Bus (ATS9350-102, Alazartech, Canada). For the in vitro experiments, the beam in the focal region was forming a light sheet across the capillary with dimensions 5 × 360 μm at full width at half maximum (FWHM).

The light sheet forming optical scheme was based on the cylindrical lens (focal length 200 mm, LJ1653L1-B-N-BK7, Thorlabs), and the objective lens (8×, NA = 0.2, Lomo, Russia) in Galilean configuration (Figure 1A). In vitro experiments were conducted in the flow cell based on the polythene fine bore capillary tube (inner diameter, 280 μm; Portex). Cell flow with an average velocity of 1.5 cm/s was formed using a motorized syringe pump AL-1000 (World Precision Instruments). Imasonic S.A. custom 3.5 MHz single element transducer (Imasonic SAS, France) with Olympus Model 5682 30 MHz preamplifier was coupled with flow cell tube by transparent medium viscosity ultrasound gel Mediagel (Geltek-Medika, Russia).

In vivo PAFC experiments were conducted by forming a 15 μm radial laser spot with LBF254-050-B (Thorlabs) objective lens. An 8 mm focused spherical symmetry ultrasonic sensor with AH-2020-025 preamplifier (ONDA) was used for acoustically limited signal detection in this case. The size of the voxel detected by the US sensor was about 50–100 μm. The voxel was aligned with the intensity maximum of the scattered laser radiation using phantoms prior to the experiment. The sensor was put into the clean water immersion tank separated with 0.6 mm transparent polyethylene dielectric film from the animal skin. An aquasonic clear ultrasound gel (Parker Laboratories) was used for coupling between the water tank and the animal skin. The detection region was chosen on the mouse femoral artery. The syringe pump AL-1000 (World Precision Instruments) was used for cell injection into the animal carotid artery with a constant speed.

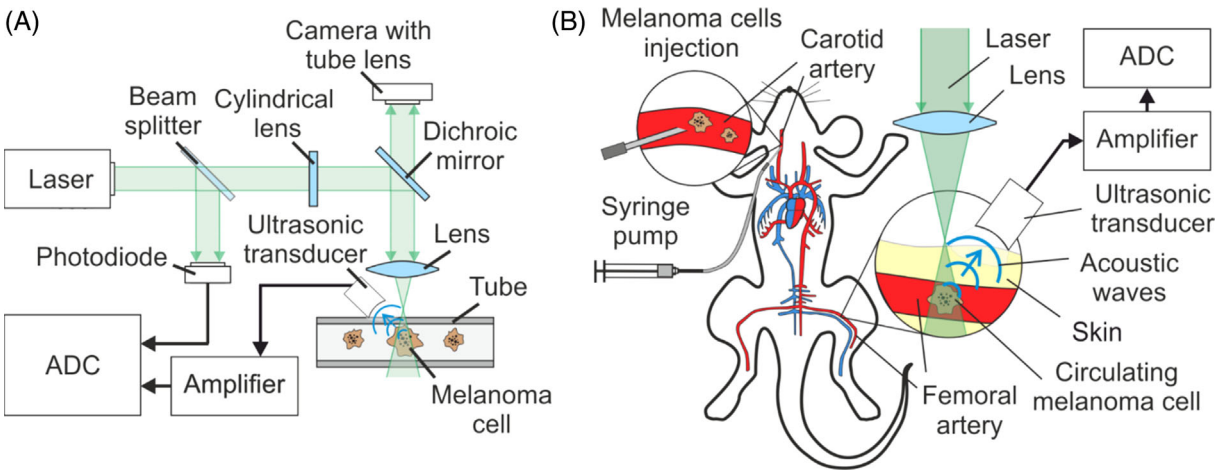

FIGURE 1 Schematic of PAFC device used to measure cell responses in vitro (A) and schematics of in vivo PAFC measurement in mice (B). [Color figure can be viewed at wileyonlinelibrary.com]

2.2 | Cell preparation

Murine melanoma cell line (B16F10) was provided by the Education and Research Institute of Nanostructures and Biosystems, Saratov State University, Russia. The cells were cultivated in Dulbecco's modified Eagle medium (DMEM) contained 4500 mg/L glucose (Sigma Aldrich) supplemented with 10% of fetal bovine serum (FBS) and 1% of penicillin–streptomycin solution (5000 U/mL) (Thermo Fisher Scientific) at 37°C in a humidified atmosphere of 5% CO_2 in the air. The media was replaced every 3 days.

Before the experiment, the cells were detached by 0.05% trypsin–EDTA solution (Thermo Fisher Scientific) and enumerated by the Countess automated cell counter (Invitrogen). Then, the cells were suspended in 1× PBS solution at a concentration of 10^7 cells per mL for absorption spectra measurements and 5×10^5 cells per mL for PA measurements. An absorption spectrum of B16F10 cells suspension was measured in the range from 300 nm to 999 nm with the 25 nm step by multi-mode microplate reader Synergy H1 (BioTek). The light absorption of cells was measured on the first, third, and fifth days of cultivation. For PA measurements, the cells were cultivated for five days to achieve the required pigmentation.

2.3 | Confocal laser scanning microscopy

The B16F10 cells, attached to the Petri dish with a glass-bottom covered by poly-L-lysine, were investigated by confocal laser scanning microscopy (CLSM). The cells were stained by Calcein AM (C1359, Sigma Aldrich, Germany), DAPI (62,248, Thermo Scientific), and MitoTracker (M7512, Invitrogen) cell dyes. Calcein AM was added to the culture media for the cell staining in proportion 1:1000 (incubation time, 30 min). After washing with DPBS, the MitoTracker red solution was added to the culture media up to the 200 nM concentration to stain the mitochondria of the adherent cells. Finally, after one more washing step, 1:1000 DAPI solution in DPBS was added to the cells and left for 10 min for cell nuclei staining with the following washing.

2.4 | Murine model

In vivo experiments were performed with Balb/c mice (6–8 weeks old, 20–25 g) provided by V.I. Razumovsky Saratov State Medical University. Animal care and all experiments were carried out according to the rules of V.I. Razumovsky Saratov State Medical University (wide approval No. 5; dated December 29, 2018). All experimental procedures were performed using general anesthesia, intraperitoneal injection of drugs (a mixture of Zoletil [40 mg per kg, 50 µL, Virbac SA, Carros, France], and 2% Rometar [10 µL and 10 mg per kg, Spofa, Czech Republic]). At the end of the experiment, animals were sacrificed by overdose of anesthesia.

To simulate CTCs in the mouse bloodstream, the B16F10 cell suspension was injected through the carotid artery using a thin polyethylene catheter (PU tubing, 32ga/.8Fr, 0.005 × 0.010 in, Instech). The catheter was implanted by the method described before [54]. This method was chosen to avoid the passive accumulation of most cells in the lungs during the first passage and increase their concentration in the vessels of other organs and tissues. Such passive accumulation is typical for cells [55, 56] and other micron-sized objects [57] after intravenous administration. Our previous works have shown that intra-arterial injection of micron-sized objects into the bloodstream allows to direct them to the region of interest more efficiently [58, 59].

The cell suspension in concentration 10^6 cells/mL was injected uniformly and slowly using the automatic syringe pump at a 40 µL/min flow rate with constant shaking of the remaining liquid. Throughout the experiment, the mouse was lying on its back and an ultrasound sensor has been positioned over the femoral artery where circulating B16F10 cells were detected. The paw used in PAFC measurement was extended diagonally to the body's position, and cotton wool was put under it. Ultrasonic clear gel (Aquasonic clear, Parker Laboratories) was applied to provide acoustic contact between skin and sensor. The PA signals from the femoral artery were continuously recorded for 10 min.

Thermal imaging in animal experiments was performed with RGK TL-80 thermal camera (RGK, China) (Figure S1).

2.5 | Signal analysis

Source files for analysis are raw PA signal waveforms measured with the 500 MSPS sample rate, 4096 samples per waveform. Waveforms are filtered by a conservative low-pass filter removing high-frequency noise from it and keeping the pulse responses from the cells. The area of time shifts corresponding to the PA signals from the blood in the large blood vessel is selected from each waveform. The PA amplitude is calculated either as peak-to-peak amplitude or root mean squared variation of signal (RMS amplitude) from this fragment. The resulting amplitude vs. time of laser pulse arrival graphs (PA traces) are plotted afterward, and all further analysis is made with these traces. A histogram of amplitudes calculated from the complete measurement sequence is calculated, and the noise level and signal detection threshold are estimated from this histogram. To find the noise level of the ultrasonic system, the short sequence of signals is recorded with a laser closed by the shutter. The signal variation from the blood flow without melanoma cells is used to estimate the detection threshold. In blood vessel in vivo measurements, variation of background from the hemoglobin-rich RBCs is subtracted from each amplitude value by averaging many sequential amplitudes. The signals above the threshold are selected for further analysis.

3 | RESULTS AND DISCUSSION

The aim of this work was to determine how a change in the laser pulse parameters affects the statistics of nonlinear PA signals in a stream of murine melanoma cells during PAFC measurement. In this work, two main laser parameters were varied, which could be controlled: the pulse width and the pulse repetition rate. For each set of parameters,

the dependence of the statistical parameters of the PA signals on the pulse energy was estimated. The primary measurable quantity is PA signal amplitude. Since a singular nonlinear signal has a random amplitude, we investigate the probability of generating high-intensity nonlinear PA signals and the statistical parameters of their amplitude distribution. This dependence was measured first in vitro for the flow in the clear capillary cell (without a strong scattering of light by biotissue) and then in vivo in the large vessels of the mouse paw with the scattering typical for this tissue depth. In the case of the capillary, we used an optically confined detection area in the form of a light sheet covering the cross-section of the capillary vessel. During the in vivo experiment, an acoustically confined small volume located approximately in the center of the vessel cross-section was used for the measurement.

The general scheme of the experiment to investigate the dependence of the statistical properties of the PA signals on the laser pulse parameters in the flow cell is shown in Figure 2A. Since the distribution of melanin particles within the cell is unique for each cell

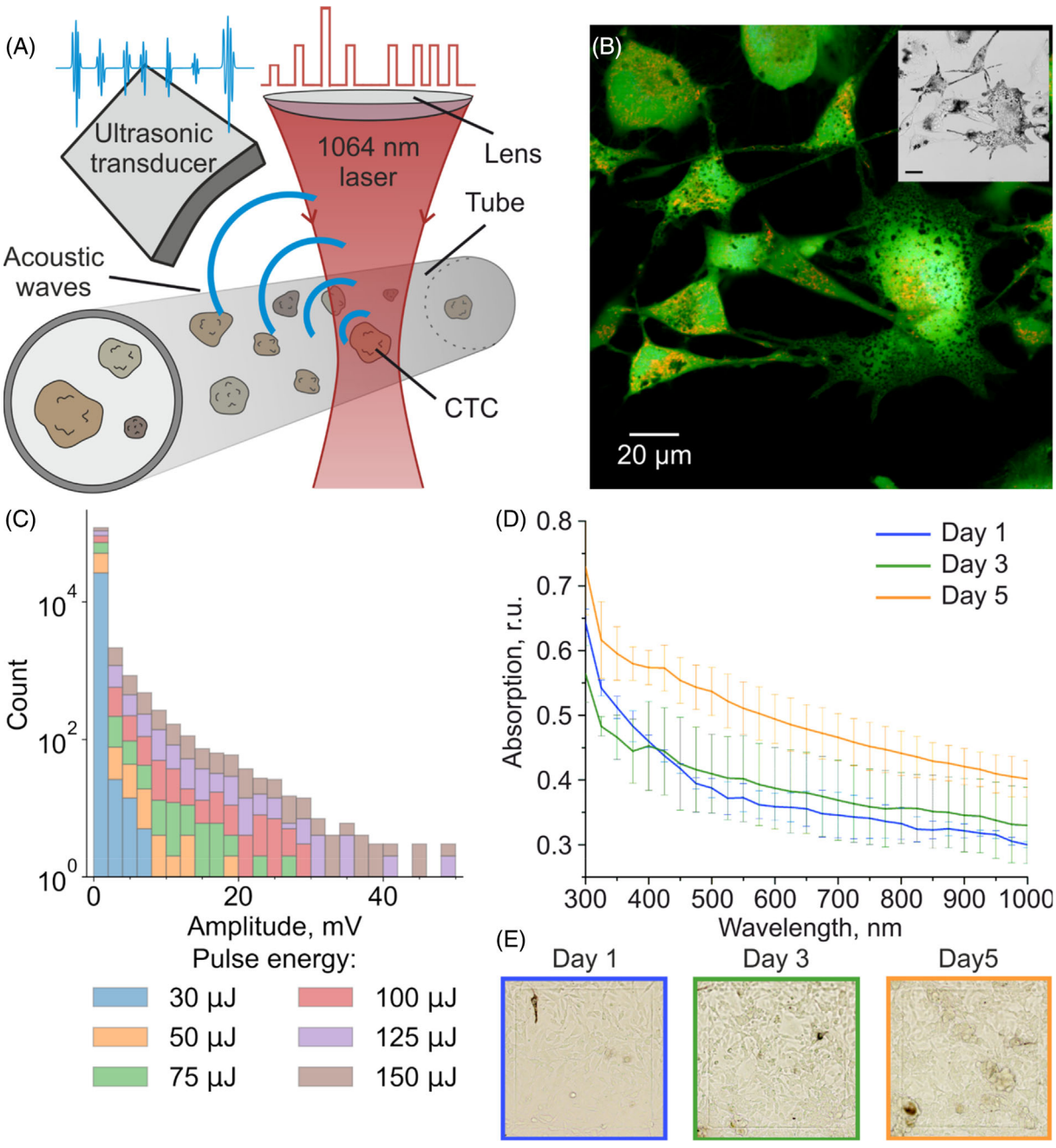

FIGURE 2 Scheme of the experiment (A): the tube with CTCs is irradiated using a laser with varying pulse parameters, forming PA signals recorded by an US transducer. Confocal microscopy of B16F10 murine melanoma cells (B); statistical parameters of PA signals from cells in the flow (C); dependencies of the B16F10 cells absorption on the day of cultivation (D); bright field images of attached B16F10 cells (E). Error bars (D) correspond to a standard deviation between three samples. [Color figure can be viewed at wileyonlinelibrary.com]

(Figure 2B), we examined the statistical distribution of a large number of PA signals (Figure 2C). In addition, we found that the distribution and concentration of melanin particles in cells strongly depend on cultivation time. The absorption of B16F10 cell suspension increased around 1.5 times from the first to fifth day of cultivation (Figure 2D). We took cells on the same cultivation day in all experiments to exclude its possible influence on the size of the melanin grains and on the optical properties of cells.

After the pulse energy exceeds a certain threshold (15–30 μJ in our experiment; Figure S2), peaks corresponding to high-amplitude nonlinear signals begin to appear on the dependences of the PA signal amplitude on time (traces). The dependencies of the amplitudes and the number of detected PA signals on the energy of laser pulses with a change in the pulse width and pulse repetition rate are shown in Figure 3. The number of detected PA signals with an amplitude above the threshold was measured. The number of signals is growing nonlinearly with increasing pulse energy. With the decreasing pulse width, the maximum amplitude is generally higher for 1 ns than 2 and 5 ns. The average amplitude of signals above the threshold is almost the same as the pulse width changes if the other parameters remain the same. The number of detected signals above the threshold increases as pulses get shorter. With the increase of pulse repetition rate from 2 to 10 kHz, the maximum amplitude has some random behavior (Figure 3C). With increasing repetition rate, the average amplitude decreases, and the number of signals increases. We consider a group of adjacent high-energy PA responses as a single melanoma cell.

It should be noted that both dependencies of the pulse amplitudes and the number of detected PA signals demonstrate a visible threshold. Below this threshold scarce and weak signals are observed,

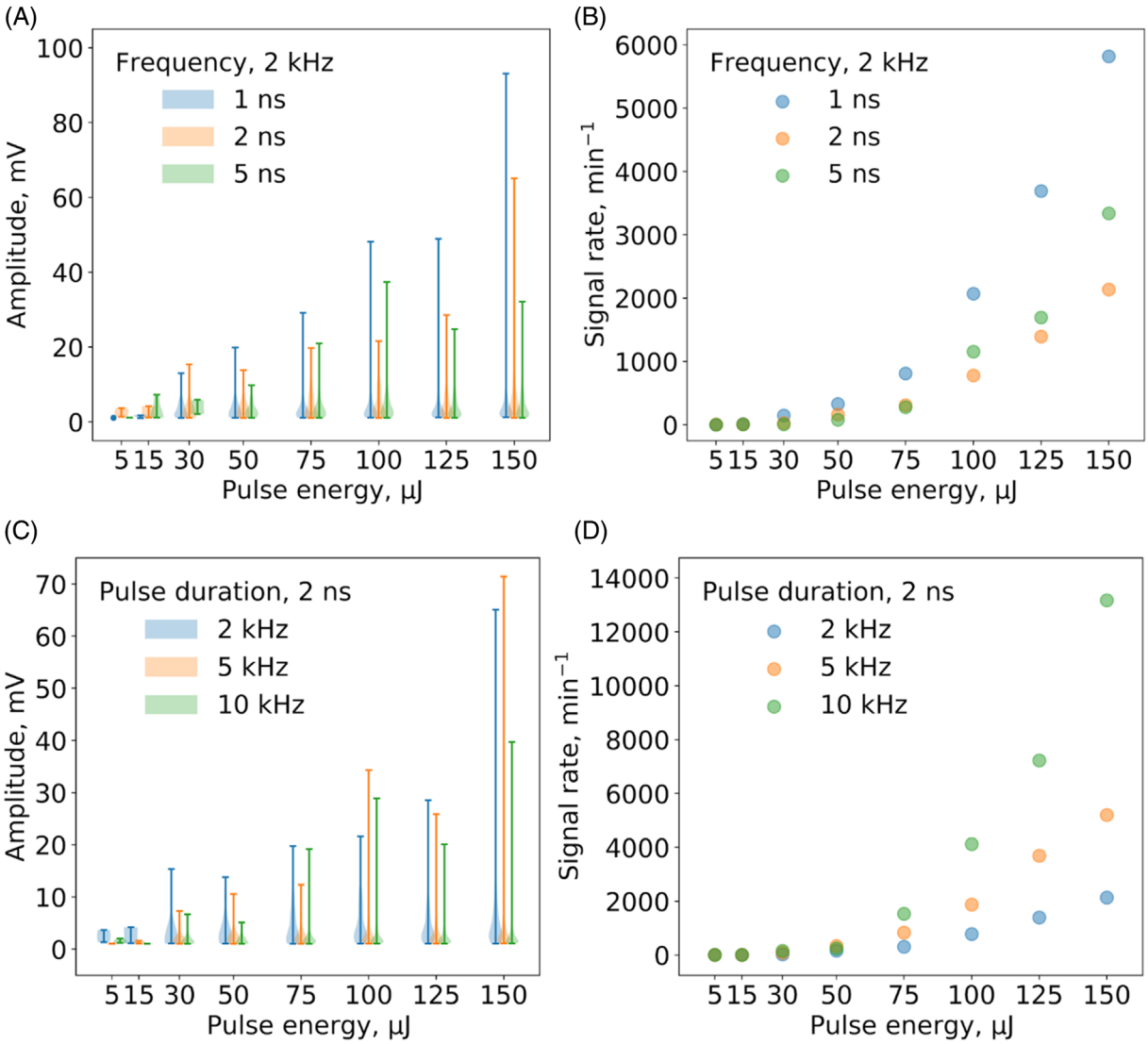

FIGURE 3 Dependences of the amplitude of the PA signals on the pulse energy at pulse widths of 1, 2, and 5 ns (A) and at frequencies of 2, 5, 10 kHz (C); dependences of the number of detected signals above the background ones on the pulse energy at widths of 1, 2, 5 ns (B) and at frequencies of 2, 5, 10 kHz (D). The violin plots' (A, C) whiskers correspond to the range of values from minimum to maximum. The violin plots' body illustrates the signal distribution. [Color figure can be viewed at wileyonlinelibrary.com]

presumably from highly pigmented aggregates. After this threshold a large number of high-amplitude signals appears. The laser beam profile in the PAFC measurement was a light sheet with a thickness of 5 μm and a length of 350 μm. The threshold energy value required for the generation of high-intensity signals for all sets of parameters lies in the pulse energy range of 30 μJ that corresponds to the energy mean fluence 0.96 J/cm^2.

The complex nature of the statistics of PA signals from B16F10 cells required a more thorough analysis. The signal intensity histogram (Figure 2C) shows a highly asymmetric distribution, and it is challenging to distinguish low-intensity signals from noise. The number of detected PA signals and their average parameters also strongly depend on the choice of the noise threshold during in vitro measurements. Some works aimed to solve this problem by analyzing the PA signal itself [44, 60] and comparing parameters of high-intensity signals and random noise [61]. In this study, as a good enough solution, the threshold was determined using a distribution of signals from an empty test tube at the "empty" part of the trace in between the high-intensity signals. If an empty part of the trace was not observed and the high-intensity signals followed too close to each other without a gap between them, the threshold was chosen by a linear approximation of the threshold dependence on the laser pulse power from the lower energies part of the graph.

Further experiments were carried out on large mouse vessels in the in vivo PAFC mode. We have succeeded in developing a device that provides reliable detection of melanoma cells in the animal paw vessels after upstream arterial injection. This approach made it possible for us to investigate the parameters of PAFC signal generation directly in the vessel of a laboratory animal during detection in an acoustically limited voxel. To achieve that, we used a focused high-frequency ultrasonic sensor with a detected voxel size of ~100 μm.

For in vivo measurements, we used a configuration of a PAFC setup with a spot illumination of 20 μm in diameter at the skin surface and an ultrasonic sensor with spherical symmetry. The measurements were carried out on the arterial or venous vessel of the BALB mouse femur by slowly injecting B16F10 cells suspension with a concentration of 10^6 cells/mL through a catheter inserted into the carotid artery. Since the intensity of the signals depends on the vessel's depth under the skin, and the number of flowing cells depends on the branching of the blood vessels in each particular animal, the measurements were carried out three times on three different animals. In this case, the same cell suspension was used during the entire variation of each parameter.

The experimental traces at the three different pulse widths are shown in Figure 4. The typical oscillograms of baseline blood flow without the melanoma cells are shown with blue color, and the oscillograms of high-intensity signals from circulating melanoma cells (CMCs) are shown with the red color. Traces with the signals from CMCs are shown in black at the right part of the figure. The places where each oscillogram is taken are shown with the red and blue vertical lines.

The waveforms of the most intense signals, undoubtedly belonging to the injected cells, are shown in Figure S3. It can be noted that the most intense signals, in addition to the central peak (the range of ultrasonic signal time delays is shown in dark gray in Figure S3), usually have a second peak, the time shift of which can differ significantly in time (the range of shifts is depicted by the light gray background in Figure S3). The dependence of the PA signal amplitude on time, shown in the inset in Figure S3 and plotted for these two ranges. It can be noted that the second peak appears for the most intense signals in the first detection range, but not all signals from the first range are accompanied by it.

The dependence of the number of detected signals and the statistics of the signal amplitude in the first time-delay range (that shown in dark gray in Figure S3) for three measurements on different animals are shown in Figure 5. It should be noted that, although the detection parameters differ significantly from animal to animal, the total number of detected cells is practically independent of the laser parameters and is reproduced with good stability. It is determined solely by the number of pigmented cells entering the desired vessel when injected upstream. It also possibly depends on the position of the detection region inside the vessel since it does not cover the entire vessel. The maximum intensity and the average intensity become noticeably higher with a pulse width of 1 ns than 2 and 5 ns; the difference between the latter two options is not noticeable. Thus, it can be noted that shorter pulses give more intense signals than longer ones, but at the same time, almost the same number of cells is detected for any pulse width in the nanosecond range.

The dependence of the strong signals number and distribution of the signal amplitude during detection directly in the mouse paw is shown in Figure 6. The number of detected signals increases with an increase of laser pulse energy. The maximum and average amplitudes also increase with increasing pulse energy, reaching, however, saturation at high energies.

The operation of PAFC is based on the fact that melanin grains that absorb more strongly at a given wavelength generate a nonlinear signal, significantly overheating compared to the environment. This allows one to see the signal from relatively small (submicron [51], micron) melanin grains, which contain much less light-absorbing substance in the detected volume than the erythrocytes surrounding this cell. As can be seen from Figure 3, there is a certain minimum energy density threshold, below which nonlinear photoacoustic signals are practically not detected. When this threshold is exceeded, both the number of signals and their average amplitude increase. It can be assumed that with an increase in the energy density required to generate nonlinear PA signals, overheating occurs in less pigmented cells. A shorter pulse duration or a higher pulse repetition rate in most cases leads to a more efficient heating of melanin grains, respectively, single pulses and a sequence of pulses, between which thermal heating does not have time to relax.

The first aspect to consider is that we need to provide a high-energy density at the vessel's depth to effectively detect melanoma cells while avoiding laser damage to cells and tissues. The primary source of damage is the absorption of light by melanin in the skin and hemoglobin (it can be present in two different variants, differing in absorption spectra depending on oxygenation). In human experiments,

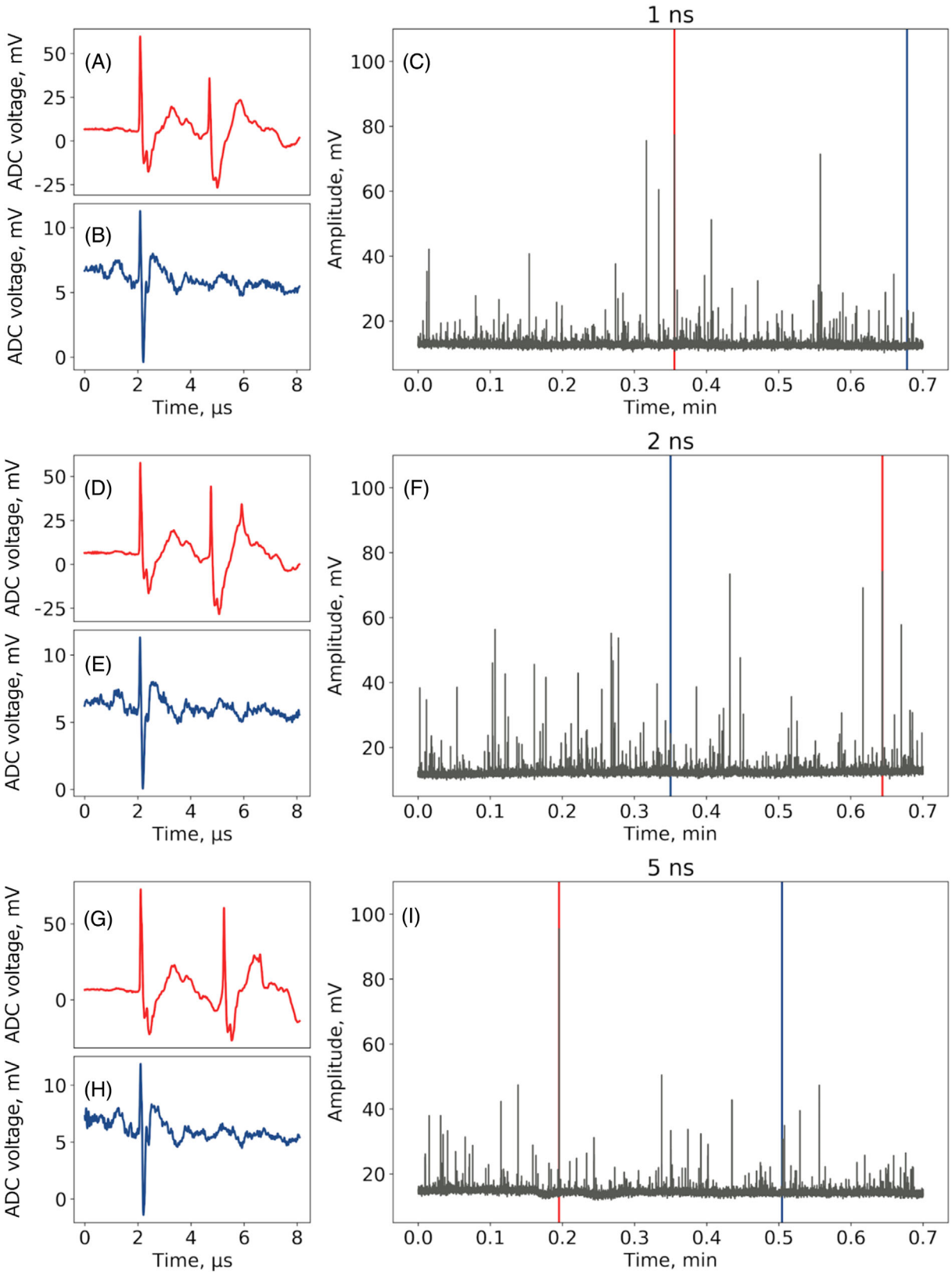

FIGURE 4 The traces from the CMC model in the mouse bloodstream after the injection are registered with 1 ns (C), 2 ns (F), and 5 ns (I) pulse widths. Red and blue lines (C, F, I) correspond to maximum amplitude and randomly selected baseline amplitude, respectively. The waveforms (A, B, D, E, G, H) correspond to data points indicated on traces. [Color figure can be viewed at wileyonlinelibrary.com]

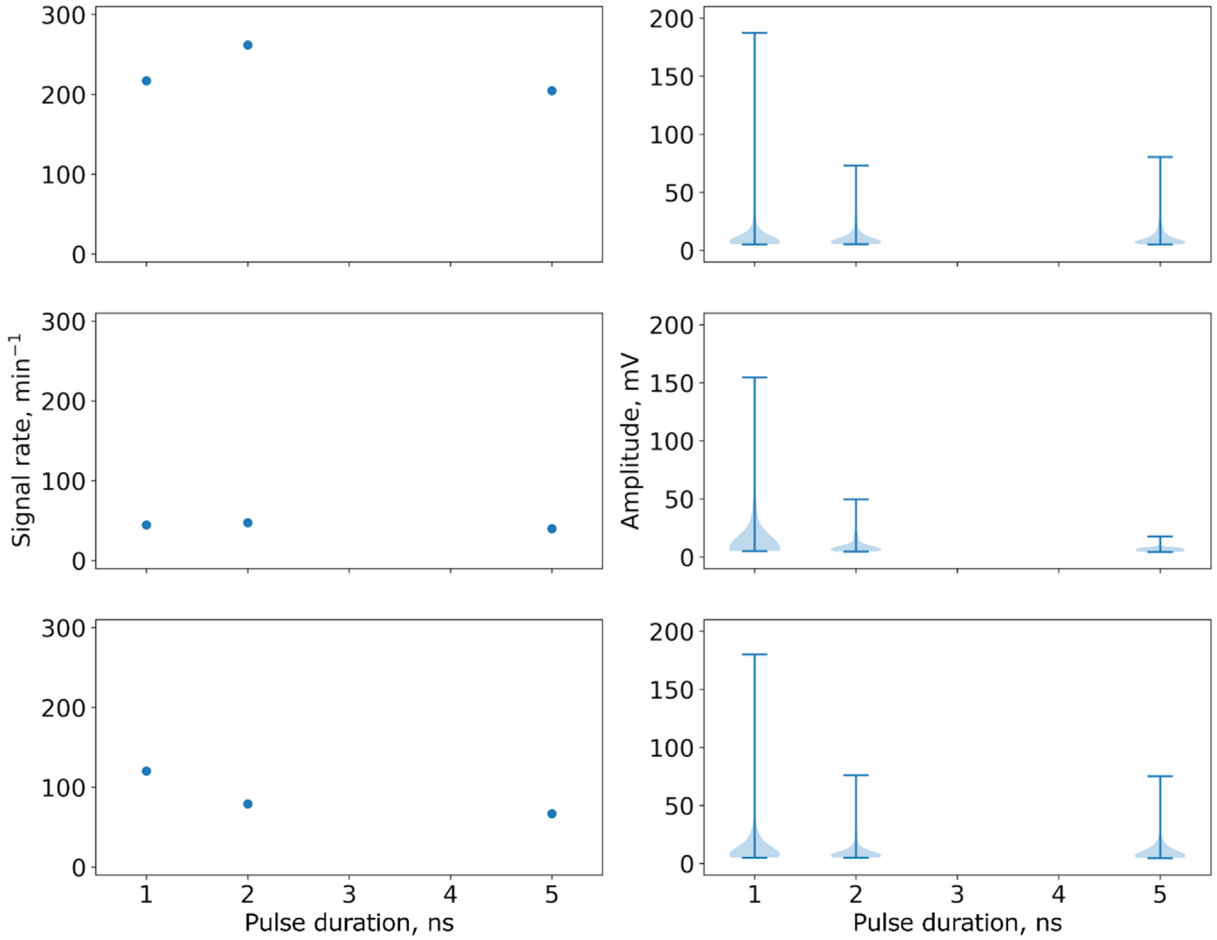

FIGURE 5 Dependence of the number of detected signals and the distribution of their amplitude at different laser pulse widths. The violin plot (right) whiskers correspond to the range of values from minimum to maximum. The violin plot body illustrates the signal distribution. [Color figure can be viewed at wileyonlinelibrary.com]

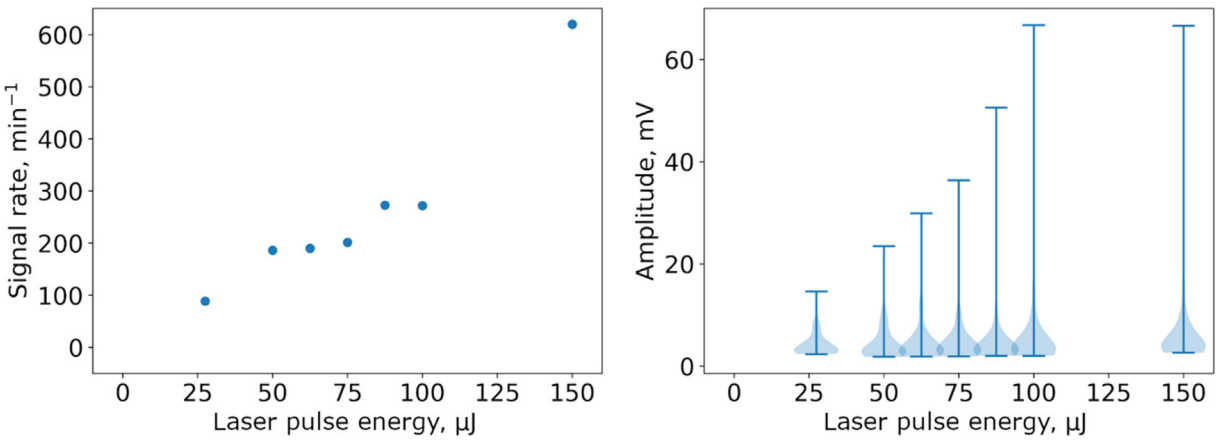

FIGURE 6 Dependence of the number of detected signals and the distribution of their amplitude at different laser pulse energies. [Color figure can be viewed at wileyonlinelibrary.com]

we must be guided by laser safety standards that prohibit using a power density greater than 1 W/cm^2 at a wavelength of 1064 nm.

The next aspect that must be taken into account is the minimum pulse repetition rate, which ensures the detection of melanoma cells at a vessel's depth. The real CTCs found in the patient has size of the order of 10–20 μm. The laser beam at a vessel's depth in laboratory animals expands to a size of 150–200 μm. Detection length is the approximately same size. At a typical blood flow velocity in the vessels

of the animal's paws of 1–2 cm/s, the time of flight of blood flow objects in the detection area will be about 10 ms, which sets the minimum required pulse repetition rate for reliable detection to be around 100 Hz. Typical laser systems with a nanosecond-range pulse length and a required pulse energy level have a pulse repetition rate of 1 kHz. With such repetition rates, about 10 pulses should come to a single cell (in our experiments, we observed from 4 to 20 that were taken into account in the subsequent analysis).

The use of energy higher than allowed for humans in mouse experiments is somewhat controversial. On the other hand, numerous reports show that the safety limit for skin damage is set too low for this type of laser system. The damage limit reported in articles is about 0.5–1 J/cm^2 for melanosomes as the primary source of photodamage of pigmented skin [48, 49]. As far as we can see, the laser parameters used in these experiments do not harm the mouse's skin (Figure S1). The temperature rise measured after prolonged exposure (15 min) does not exceed 8°C (Figure S1C) if the ultrasonic-coupling water bath is in contact with skin. Without the water container working as a cooler in this case, the skin temperature rises to 42°C (Figure S1A) in the local spot of laser irradiation.

An increase in the equilibrium temperature in the medium results in an increase in the Gruneisen coefficient, and thus the PA signal amplitude (estimated ∼5% per 1°C) [62]. As the maximum increase of temperature is ∼8°C (Figure S1C) with water tank cooling the skin, the estimated increase of volume Gruneisen coefficient should be ∼35% in this case at skin level. Local overheating of melanin grain provides a large local increase of the Gruneisen coefficient and PA signal from the grain.

At the blood vessel's depth where the melanoma cells and RBCs are exposed to laser light, our estimation of beam profile diameter of the scattered beam is 150–200 μm. In addition, some attenuation of energy is caused by light absorption by the skin pigmentation and small blood vessels under the skin. It is known that melanosomes damage starts at energy ∼500 mJ/cm^2 (micro cavitation threshold defined in Reference [63]) that is not achievable at the vessel's depth, and the extinction coefficients of melanin are already measured with these laser energies.

Nonetheless, either burn, irritation, or some pain effects are not seen even with the harshest combination of parameters used in this article. There should be neither pigment spots nor remaining hair in the laser-irradiated area, otherwise, no damage is not guaranteed; we ensure this by taking a navigation camera image before turning the laser on. It should be noted that blood flow in the vessel is somewhat crucial for effective cooling of the skin resulting in no damage. The skin above the vessel does not overheat with prolonged exposure, and the skin without a large vessel underneath it overheats in a couple of minutes with the high-energy-high repetition rate combination of parameters. From our prior experience, PA signals can also show signs of skin overheating at early stages. High amplitude short-time spike from the overheated melanin-rich layer of skin appears on waveforms at less time-shift then the signal from the vessel provided by hemoglobin contrast. We have not seen such signals during the experimental procedure or in our experimental data.

4 | CONCLUSIONS

The murine model of CTCs that provides the constant flow of large numbers of similar melanoma cells in the mouse blood was introduced. By measuring a large ensemble of cells, we estimated how a variation of the laser parameters affects the statistics of PA signals. The study was carried out both for the cell suspension flow in vitro and for cells injected into the bloodstream of immunocompetent mice in vivo. The effect of laser pulse width, repetition rate, and pulse energy on the statistics of signals from melanoma cells was investigated. We have studied how the PA amplitude changes during the PAFC measurements, including heating the measured volume, natural blood flow variations, and other effects from in vivo measurement conditions. With a change in the laser pulse width from 5 to 1 ns, an increase in the average and maximum amplitudes of PA signals was observed without a noticeable change in the number of high-intensity signals. As the pulse energy density in the flow cell increases, the number of detected signals increases, and the average and maximum amplitudes of the signals (reach saturation at some pulse energy density). It was shown that the energy density makes the main contribution to the efficiency of cell detection in the bloodstream at a vessel's depth.

AUTHOR CONTRIBUTIONS

Ekaterina S. Prikhozhdenko: Formal analysis; data curation; writing – review and editing; visualization. **Oleg V. Grishin:** Validation; investigation; data curation; writing – original draft. **Natalia A. Shushunova:** Validation; investigation; writing – original draft. **Daniil N. Bratashov:** Conceptualization; methodology; software; formal analysis; writing – original draft; writing – review and editing; supervision; project administration. **Roman A. Verkhovskii:** Investigation; writing – original draft; visualization. **Anastasiia A. Kozlova:** Software; investigation; data curation; writing – original draft; visualization. **Arkady S. Abdurashitov:** Investigation; software. **Olga A. Sindeeva:** Methodology; writing – review and editing; funding acquisition. **Anatoly S. Karavaev:** Software. **Danil D. Kulminskiy:** Software. **Evgeny V. Shashkov:** Validation; resources. **Olga A. Inozemtseva:** Resources; writing – original draft; writing – review and editing; supervision; project administration; funding acquisition. **Valery V Tuchin:** Resources; writing – review and editing; supervision.

ACKNOWLEDGMENTS

This work was supported by the Government of the Russian Federation (grant number 14.Z50.31.0044 to support scientific research projects implemented under the supervision of leading scientists at Russian institutions and Russian institutions of higher education). Olga A. Sindeeva acknowledges the Grant of the President of Russian Federation (MK-4273.2021.1.4) for supporting the preliminary studies aimed to find the optimal way of cell injection into the bloodstream.

FUNDING INFORMATION

This research was funded by the Government of the Russian Federation, grant number 14.Z50.31.0044. Olga A. Sindeeva acknowledges

the Grant of the President of Russian Federation (MK-4273.2021.1.4) for supporting the preliminary studies aimed to find the optimal way of cell injection into the bloodstream.

CONFLICT OF INTEREST STATEMENT

The authors declare no conflict of interest.

DATA AVAILABILITY STATEMENT

The data presented in this study are available on request from the corresponding author. The data are not publicly available due to the large volume of PAFC data files.

ORCID

Oleg V. Grishin https://orcid.org/0000-0001-7463-6536
Natalia A. Shushunova https://orcid.org/0000-0001-5366-1783
Daniil N. Bratashov https://orcid.org/0000-0002-2096-4478
Ekaterina S. Prikhozhdenko https://orcid.org/0000-0003-2700-168X
Roman A. Verkhovskii https://orcid.org/0000-0003-1830-4582
Anastasiia A. Kozlova https://orcid.org/0000-0002-9336-0317
Arkady S. Abdurashitov https://orcid.org/0000-0003-0731-8364
Olga A. Sindeeva https://orcid.org/0000-0002-5288-4157
Anatoly S. Karavaev https://orcid.org/0000-0003-4678-3648
Danil D. Kulminskiy https://orcid.org/0000-0002-3936-2813
Evgeny V. Shashkov https://orcid.org/0000-0003-0920-6366
Olga A. Inozemtseva https://orcid.org/0000-0002-8898-8169
Valery V. Tuchin https://orcid.org/0000-0001-7479-2694

REFERENCES

1. Steenbergen W, Zharov VP. Towards reaching the total blood volume by in vivo flow cytometry and theranostics. Cytometry Part A. 2019; 95:1223–5. https://doi.org/10.1002/cyto.a.23916
2. Tuchin VV, Tárnok A, Zharov VP. In vivo flow cytometry: a horizon of opportunities. Cytometry Part A. 2011;79A:737–45. https://doi.org/10.1002/cyto.a.21143
3. Tuchin VV. In vivo optical flow cytometry and cell imaging. Riv Nuovo Cimento. 2014;37:375–416. https://doi.org/10.1393/ncr/i2014-10102-x
4. Suo Y, Gu Z, Wei X. Advances of in vivo flow cytometry on cancer studies. Cytometry Part A. 2020;97:15–23. https://doi.org/10.1002/cyto.a.23851
5. Theil G, Fischer K, Weber E, Medek R, Hoda R, Lücke K, et al. The use of a new cellcollector to isolate circulating tumor cells from the blood of patients with different stages of prostate cancer and clinical outcomes – a proof-of-concept study. PLoS One. 2016;11:e0158354. https://doi.org/10.1371/journal.pone.0158354
6. Zhu X, Suo Y, Ding N, He H, Wei X. Circulating tumor cells occur non-uniformly monitored by in vivo flow cytometry. Proceedings of the international conference on photonics and imaging in biology and medicine. Washington, D.C: OSA; 2017. W3A.104.
7. Patil R, Tan X, Bartosik P, Detappe A, Runnels JM, Ghobrial I, et al. Fluorescence monitoring of rare circulating tumor cell and cluster dissemination in a multiple myeloma xenograft model in vivo. J Biomed Opt. 2019;24:1–11. https://doi.org/10.1117/1.JBO.24.8.085004
8. Galanzha EI, Menyaev YA, Yadem AC, Sarimollaoglu M, Juratli MA, Nedosekin DA, et al. In vivo liquid biopsy using cytophone platform for photoacoustic detection of circulating tumor cells in patients with melanoma. Sci Transl Med. 2019;11:eaat5857. https://doi.org/10.1126/scitranslmed.aat5857
9. Galanzha EI, Zharov VP. Photoacoustic flow cytometry. Methods. 2012;57:280–96. https://doi.org/10.1016/j.ymeth.2012.06.009
10. He G, Xu D, Qin H, Yang S, Xing D. In vivo cell characteristic extraction and identification by photoacoustic flow cytography. Biomed Opt Express. 2015;6:3748–56. https://doi.org/10.1364/BOE.6.003748
11. Jawad HJ, Yadem AC, Menyaev YA, Sarimollaoglu M, Armstrong JN, Watanabe F, et al. Towards rainbow portable Cytophone with laser diodes for global disease diagnostics. Sci Rep. 2022;12:8671. https://doi.org/10.1038/s41598-022-11452-w
12. Hai P, Zhou Y, Zhang R, Ma J, Li Y, Shao J-Y, et al. Label-free high-throughput detection and quantification of circulating melanoma tumor cell clusters by linear-array-based photoacoustic tomography. J Biomed Opt. 2016;22:1. https://doi.org/10.1117/1.JBO.22.4.041004
13. Hai P, Qu Y, Li Y, Zhu L, Shmuylovich L, Cornelius LA, et al. Label-free high-throughput photoacoustic tomography of suspected circulating melanoma tumor cells in patients in vivo. J Biomed Opt. 2020;25:1–17. https://doi.org/10.1117/1.JBO.25.3.036002
14. Juratli MA, Sarimollaoglu M, Siegel ER, Nedosekin DA, Galanzha EI, Suen JY, et al. Real-time monitoring of circulating tumor cell release during tumor manipulation using in vivo photoacoustic and fluorescent flow cytometry. Head Neck. 2014;36:1207–15. https://doi.org/10.1002/hed.23439
15. Suo Y, Liu T, Xie C, Wei D, Tan X, Wu L, et al. Near infrared in vivo flow cytometry for tracking fluorescent circulating cells. Cytometry Part A. 2015;87:878–84. https://doi.org/10.1002/cyto.a.22711
16. Fan Z-C, Yan J, Liu G-D, Tan X-Y, Weng X-F, Wu W-Z, et al. Real-time monitoring of rare circulating hepatocellular carcinoma cells in an orthotopic model by in vivo flow cytometry assesses resection on metastasis. Cancer Res. 2012;72:2683–91. https://doi.org/10.1158/0008-5472.CAN-11-3733
17. Nolan J, Nedosekin DA, Galanzha EI, Zharov VP. Detection of apoptotic circulating tumor cells using in vivo fluorescence flow cytometry. Cytometry Part A. 2019;95:664–71. https://doi.org/10.1002/cyto.a.23642
18. Novak J, Georgakoudi I, Wei X, Prossin A, Lin CP. In vivo flow cytometer for real-time detection and quantification of circulating cells. Opt Lett. 2004;29:77–9. https://doi.org/10.1364/OL.29.000077
19. Lee H, Alt C, Pitsillides CM, Puoris'haag M, Lin CP. In vivo imaging flow cytometer. Opt Express. 2006;14:7789–800. https://doi.org/10.1364/OE.14.007789
20. Verkhovskii RA, Kozlova AA, Sindeeva OA, Kozhevnikov IO, Prikhozhdenko ES, Mayorova OA, et al. Lightsheet-based flow cytometer for whole blood with the ability for the magnetic retrieval of objects from the blood flow. Biomed Opt Express. 2021;12:380–94. https://doi.org/10.1364/BOE.413845
21. Markovic S, Li B, Pera V, Sznaier M, Camps O, Niedre M. A computer vision approach to rare cell in vivo fluorescence flow cytometry. Cytometry Part A. 2013;83:1113–23. https://doi.org/10.1002/cyto.a.22397
22. Markovic S, Li S, Niedre MJ. Performance of computer vision in vivo flow cytometry with low fluorescence contrast. J Biomed Opt. 2015; 20:1. https://doi.org/10.1117/1.JBO.20.3.035005
23. He W, Wang H, Hartmann LC, Cheng J-X, Low PS. In vivo quantitation of rare circulating tumor cells by multiphoton intravital flow cytometry. Proc Natl Acad Sci. 2007;104:11760–5. https://doi.org/10.1073/pnas.0703875104
24. Golan L, Yeheskely-Hayon D, Minai L, Dann EJ, Yelin D. Noninvasive imaging of flowing blood cells using label-free spectrally encoded flow cytometry. Biomed Opt Express. 2012;3:1455–64. https://doi.org/10.1364/BOE.3.001455

25. Xie L, Yang Y, Sun X, Qiao X, Liu Q, Song K, et al. 2D light scattering static cytometry for label-free single cell analysis with submicron resolution. Cytometry Part A. 2015;87:1029–37. https://doi.org/10.1002/cyto.a.22713
26. Greiner C, Hunter M, Rius F, Huang P, Georgakoudi I. Confocal backscattering-based detection of leukemic cells in flowing blood samples. Cytometry Part A. 2011;79A:874–83. https://doi.org/10.1002/cyto.a.21086
27. Vora N, Shekhar P, Esmail M, Patra A, Georgakoudi I. Label-free flow cytometry of rare circulating tumor cell clusters in whole blood. Sci Rep. 2022;12:10721. https://doi.org/10.1038/s41598-022-14003-5
28. Pace J, Ivich F, Marple E, Niedre M. Near-infrared diffuse in vivo flow cytometry. J Biomed Opt. 2022;27:27. https://doi.org/10.1117/1.JBO.27.9.097002
29. Zettergren E, Vickers D, Runnels J, Murthy SK, Lin CP, Niedre M. Instrument for fluorescence sensing of circulating cells with diffuse light in mice in vivo. J Biomed Opt. 2012;17:037001. https://doi.org/10.1117/1.JBO.17.3.037001
30. Pera V, Tan X, Runnels J, Sardesai N, Lin CP, Niedre M. Diffuse fluorescence fiber probe for in vivo detection of circulating cells. J Biomed Opt. 2017;22:037004. https://doi.org/10.1117/1.JBO.22.3.037004
31. Tan X, Patil R, Bartosik P, Runnels JM, Lin CP, Niedre M. In vivo flow cytometry of extremely rare circulating cells. Sci Rep. 2019;9:3366. https://doi.org/10.1038/s41598-019-40143-2
32. Yang W, Li A, Suo Y, Lu F-K, Sunney Xie X. Simultaneous two-color stimulated Raman scattering microscopy by adding a fiber amplifier to a 2 ps OPO-based SRS microscope. Opt Lett. 2017;42:523–6. https://doi.org/10.1364/OL.42.000523
33. Han M, Watts JA, Jamshidi-Parsian A, Nadeem U, Sarimollaoglu M, Siegel ER, et al. In vivo lymphatic circulating tumor cells and progression of metastatic disease. Cancers. 2020;12:2866. https://doi.org/10.3390/cancers12102866
34. Sindeeva OA, Verkhovskii RA, Sarimollaoglu M, Afanaseva GA, Fedonnikov AS, Osintsev EY, et al. New frontiers in diagnosis and therapy of circulating tumor markers in cerebrospinal fluid in vitro and in vivo. Cell. 2019;8:1195. https://doi.org/10.3390/cells8101195
35. Galanzha E, Zharov V. Circulating tumor cell detection and capture by photoacoustic flow cytometry in vivo and ex vivo. Cancers. 2013;5:1691–738. https://doi.org/10.3390/cancers5041691
36. Juratli MA, Menyaev YA, Sarimollaoglu M, Melerzanov AV, Nedosekin DA, Culp WC, et al. Noninvasive label-free detection of circulating white and red blood clots in deep vessels with a focused photoacoustic probe. Biomed Opt Express. 2018;9:5667–77. https://doi.org/10.1364/BOE.9.005667
37. Das D, Sivasubramanian K, Rajendran P, Pramanik M. Label-free high frame rate imaging of circulating blood clots using a dual modal ultrasound and photoacoustic system. J Biophotonics. 2021;14:e202000371. https://doi.org/10.1002/jbio.202000371
38. Cai C, Nedosekin DA, Menyaev YA, Sarimollaoglu M, Proskurnin MA, Zharov VP. Photoacoustic flow cytometry for single sickle cell detection in vitro and in vivo. Anal Cell Pathol. 2016;2016:1–11. https://doi.org/10.1155/2016/2642361
39. Cai C, Carey KA, Nedosekin DA, Menyaev YA, Sarimollaoglu M, Galanzha EI, et al. In vivo photoacoustic flow cytometry for early malaria diagnosis. Cytometry Part A. 2016;89:531–42. https://doi.org/10.1002/cyto.a.22854
40. Edgar RH, Cook J, Noel C, Minard A, Sajewski A, Fitzpatrick M, et al. Bacteriophage-mediated identification of bacteria using photoacoustic flow cytometry. J Biomed Opt. 2019;24:1–7. https://doi.org/10.1117/1.JBO.24.11.115003
41. Juratli MA, Menyaev YA, Sarimollaoglu M, Siegel ER, Nedosekin DA, Suen JY, et al. Real-time label-free embolus detection using In vivo photoacoustic flow cytometry. PLoS One. 2016;11:e0156269. https://doi.org/10.1371/journal.pone.0156269
42. Choi W, Park E-Y, Jeon S, Kim C. Clinical photoacoustic imaging platforms. Biomed Eng Lett. 2018;8:139–55. https://doi.org/10.1007/s13534-018-0062-7
43. Fatima A, Kratkiewicz K, Manwar R, Zafar M, Zhang R, Huang B, et al. (Mohammad) review of cost reduction methods in photoacoustic computed tomography. Photo-Dermatology. 2019;15:100137. https://doi.org/10.1016/j.pacs.2019.100137
44. Erfanzadeh M, Zhu Q. Photoacoustic imaging with low-cost sources; a review. Photo-Dermatology. 2019;14:1–11. https://doi.org/10.1016/j.pacs.2019.01.004
45. Petrov YY, Petrova IY, Patrikeev IA, Esenaliev RO, Prough DS. Multiwavelength optoacoustic system for noninvasive monitoring of cerebral venous oxygenation: a pilot clinical test in the internal jugular vein. Opt Lett. 2006;31:1827–9. https://doi.org/10.1364/OL.31.001827
46. Zackrisson S, van de Ven SMWY, Gambhir SS. Light in and sound out: emerging translational strategies for photoacoustic imaging. Cancer Res. 2014;74:979–1004. https://doi.org/10.1158/0008-5472.CAN-13-2387
47. American national standard for safe use of lasers. Washington, USA: Laser Institute of America; 2014.
48. DeLisi MP, Peterson AM, Noojin GD, Shingledecker AD, Tijerina AJ, Boretsky AR, et al. Porcine skin damage thresholds for pulsed nanosecond-scale laser exposure at 1064-nm. In: Jansen ED, Beier HT, editors. Proceedings of the optical interactions with tissue and cells XXIX. San Francisco, CA: SPIE; 2018. p. 6.
49. Jean M, Schulmeister K. Laser-induced injury of the skin: validation of a computer model to predict thresholds. Biomed Opt Express. 2021;12:2586–603. https://doi.org/10.1364/BOE.422618
50. Sarimollaoglu M, Nedosekin DA, Menyaev YA, Juratli MA, Zharov VP. Nonlinear photoacoustic signal amplification from single targets in absorption background. Photo-Dermatology. 2014;2:1–11. https://doi.org/10.1016/j.pacs.2013.11.002
51. Kozlova A, Bratashov D, Grishin O, Abdurashitov A, Prikhozhdenko E, Verkhovskii R, et al. Dynamic blood flow phantom for in vivo liquid biopsy standardization. Sci Rep. 2021;11:1185. https://doi.org/10.1038/s41598-020-80487-8
52. Irisawa K, Hirasawa T, Hirota K, Tsujita K, Ishihara M. Influence of laser pulse width to the photoacoustic temporal waveform and the image resolution with a solid state excitation laser. Proc SPIE. 2012;8223:82232W.
53. Li C, Wang LV. Photoacoustic tomography and sensing in biomedicine. Phys Med Biol. 2009;54:R59–97. https://doi.org/10.1088/0031-9155/54/19/R01
54. Jacobs JD, Hopper-Borge EA. Carotid artery infusions for pharmacokinetic and pharmacodynamic analysis of Taxanes in mice. J Vis Exp. 2014;95:e51917. https://doi.org/10.3791/51917
55. Leibacher J, Henschler R. Biodistribution, migration and homing of systemically applied mesenchymal stem/stromal cells. Stem Cell Res Ther. 2016;7:7. https://doi.org/10.1186/s13287-015-0271-2
56. Quillien V, Moisan A, Lesimple T, Leberre C, Toujas L. Biodistribution of 111 indium-labeled macrophages infused intravenously in patients with renal carcinoma. Cancer Immunol Immunother. 2001;50:477–82. https://doi.org/10.1007/s002620100224
57. Sindeeva OA, Verkhovskii RA, Abdurashitov AS, Voronin DV, Gusliakova OI, Kozlova AA, et al. Effect of systemic polyelectrolyte microcapsule administration on the blood flow dynamics of vital organs. ACS Biomater Sci Eng. 2020;6:389–97. https://doi.org/10.1021/acsbiomaterials.9b01669
58. Mayorova OA, Sindeeva OA, Lomova MV, Gusliakov OI, Tarakanchikova YV, Tyutyaev EV, et al. Endovascular addressing improves the effectiveness of magnetic targeting of drug carrier.

Comparison with the conventional administration method. Nanomedicine. 2020;28:102184. https://doi.org/10.1016/j.nano.2020.102184

59. Prikhozhdenko ES, Gusliakova OI, Kulikov OA, Mayorova OA, Shushunova NA, Abdurashitov AS, et al. Target delivery of drug carriers in mice kidney glomeruli via renal artery. Balance between efficiency and safety. J Control Release. 2021;329:175–90. https://doi.org/10.1016/j.jconrel.2020.11.051
60. Wang Q, Pang K, Zhou Q, Yang P, He H, Wei X, et al. Improving label-free detection of circulating melanoma cells by photoacoustic flow cytometry. In: Chen WR, editor. Proceedings of the biophotonics and immune responses XIII. San Francisco, CA: SPIE; 2018. p. 29.
61. Wang Q, Zhou Q, Yang P, Wang X, Niu Z, Suo Y, et al. In: Chen WR, editor. Optimized signal detection and analysis methods for in vivo photoacoustic flow cytometry. San Francisco, CA: SPIE; 2017. 100650C.
62. Yao J, Wang LV. Sensitivity of photoacoustic microscopy. Photo-Dermatology. 2014;2:87–101. https://doi.org/10.1016/j.pacs.2014.04.002
63. Schmidt MS, Kennedy PK, Noojin GD, Vincelette RL, Thomas RJ, Rockwell BA. Trends in nanosecond melanosome microcavitation up to 1540 nm. J Biomed Opt. 2015;20:095011. https://doi.org/10.1117/1.JBO.20.9.095011

SUPPORTING INFORMATION

Additional supporting information can be found online in the Supporting Information section at the end of this article.

How to cite this article: Grishin OV, Shushunova NA, Bratashov DN, Prikhozhdenko ES, Verkhovskii RA, Kozlova AA, et al. Effect of pulsed laser parameters on photoacoustic flow cytometry efficiency in vitro and in vivo. Cytometry. 2023. https://doi.org/10.1002/cyto.a.24778